Theory of the l-state population of Rydberg states formed in ion-solid collisions

Jürgen Kemmler, Joachim Burgdörfer, and Carlos O. Reinhold
University of Tennessee, Knoxville, Tennessee 37996-1200
and Oak Ridge National Laboratory, Oak Ridge, Tennessee 37831-6377
(Received 15 April 1991)

The experimentally observed high-l-state population of ions excited in ion-solid interactions differs sharply from l-state populations produced in ion-atom collisions. We have studied the population dynamics of electronic excitation and transport within the framework of a classical transport theory for O^{2+} (2-MeV/u) ions traversing C foils. The resulting delayed-photon-emission intensities are found to be in very good agreement with experiment. Initial phase-space conditions have been obtained from both classical-trajectory Monte Carlo calculations and random initial distributions. We find evidence that the very-high-l-state populations produced in ion-solid collisions are the result of a diffusion to high-l states under the influence of multiple scattering in the bulk of the solid.

I. INTRODUCTION

Since the early days of beam-foil spectroscopy, the nonexponential decay of beam-foil-excited electronic states has been known to complicate the accurate determination of lifetimes [1]. It became clear very soon [2,3] that this behavior was caused by the cascades from highly excited states, which modify the time dependence of the photon intensity $I(t)$ for $t \gg \tau_{n,l}$ ($\tau_{n,l}$ being the lifetime of the state) from an exponential to an approximate power-law dependence $I(t) \propto t^{-a}$. Calculations of cascade contributions to the observed states showed [4,5] that fast ions emerge from the solid in Rydberg states with very high angular momenta l. This contrasts sharply with binary ion-atom collisions at similar high collision velocities in which mainly small l values are populated ($l \lesssim 1$). This observation—not easily explained in terms of conventional binary collision models—has become a standard for "solid-state effects" characterizing ion penetration through solids.

Delayed-photon-emission spectroscopy is one important tool for investigating the high-l population of Rydberg states emerging from solids. The principle of this method is to measure the cascade contribution from high-n,l states by observing the time-dependent photon flux $I(t)$ of Ly_α or Ly_β transitions for $t \gg \tau_{n,l}$. Recently, it has become possible to observe the l distribution more directly [6] by applying "angular-momentum-resolved Auger spectroscopy." However, because of the inherent requirements on the energy resolution of different l states this method is restricted to moderate-n shells.

A large body of data on high-l Rydberg-state population, mostly for highly charged ions ($Z_p \gg 1$), has been compiled in several laboratories. A theoretical analysis of these results appears to be, heretofore, missing. In the following we present a detailed study of the Ly_α and Ly_β radiation for hydrogenic O^{7+} resulting from the passage of 2-MeV/u O^{2+} ions through thick carbon foils [7]. Our analysis employs the recently developed method of classical simulation for the electronic evolution during the passage of ions through the solid [8], which has been successfully applied [9] to explain the l distribution of the $n=5$ shell of carbon observed by Yamazaki *et al.* [6]. In this work we apply this theoretical concept to the evolution of the l distribution of high Rydberg states. While our numerical results pertain to the collision system $O^{2+} \rightarrow C$, our findings provide for the first time an explanation for the production of high-l Rydberg states in other collision systems.

Special attention is focused on the initial phase-space distributions and on the effective projectile potential used in our classical transport calculations. The sensitivity of the final results with respect to the initial conditions will be tested by employing both a "random" initial distribution and an initial phase-space distribution resulting from a classical-trajectory Monte Carlo (CTMC) calculation. We will also investigate the effect of Stark mixing. Atomic units are used throughout the paper unless otherwise specified.

II. ELECTRON EXCITATION AND TRANSPORT

A. General

It is convenient to distinguish three different steps of the electronic excitation in ion-solid collisions: (i) the primary binary collision in the bulk of the target by which a bound projectile electron is excited or a target electron captured into an excited state, (ii) the transport of the excited electron towards the exit of the solid, and (iii) the solid-vacuum transition and its influence on the finally measured electronic configuration.

While highly desirable, a description in terms of quantum-mechanical transport theory is a challenging task in view of the large number of coupled states and the ambiguity in the choice of an appropriate basis set. It should be stressed that excited states in a solid have to be viewed as strongly perturbed transient wave packets with little resemblance to stationary atomic states in vacuum.

A classical transport theory [8] circumvents this prob-

lem. Its justification is in part based on the observation that the manifold of projectile bound and continuum states can be divided into two regimes separated by a critical quantum number n_c: (a) deeply bound states which are at most slightly disturbed by the multiple inelastic and elastic collisions with the electrons and atomic cores in the target, and (b) the highly excited electrons with either negative or positive binding energies in the frame of the projectile ion strongly perturbed by collisional interactions. A rough estimate of the critical n_c value separating these two regimes can be obtained from the criterion that collisional broadening exceeds the level spacing. An order-of-magnitude estimate in the case of hydrogenlike bound states gives [10]

$$n_c \simeq \left[\frac{Z_p^2 \lambda_f}{2\pi v_p} \right]^{1/3} . \tag{1}$$

Here λ_f denotes the mean free path between two collisions and Z_p and v_p are the projectile charge and velocity, respectively. For electrons in states $n > n_c$, the conventional description in terms of stationary states is no longer valid: in this case the electron cannot complete even a single orbit around the projectile ion without suffering a collision. In this regime, for which collisional interactions strongly perturb bound states, quantum effects due to the existence of a discrete spectrum can be neglected. In the framework of classical dynamics, the transport problem can be expressed in terms of a microscopic Langevin equation of motion for the momentum vector $\mathbf{p}_e$ of the electron [8]

$$\frac{d\mathbf{p}_e}{dt} = -\nabla V_p + \mathbf{F}(t) . \tag{2}$$

This equation describes the motion of the electron in a classical orbit in an effective electron-projectile potential, perturbed by a random force $\mathbf{F}(t)$ which represents the inelastic and elastic collisions the electron suffers in the solid. In order to test the sensitivity of the results to the form of the potential, we have analyzed in this work two particular forms: a dynamically screened potential ($V_p^{(s)}$) obtained from linear response theory [11] and a bare Coulomb potential $V_p^{(b)}$. The screened potential is anisotropic ("wake," Fig. 1) which leads to a Stark splitting of bound states in the solid [12].

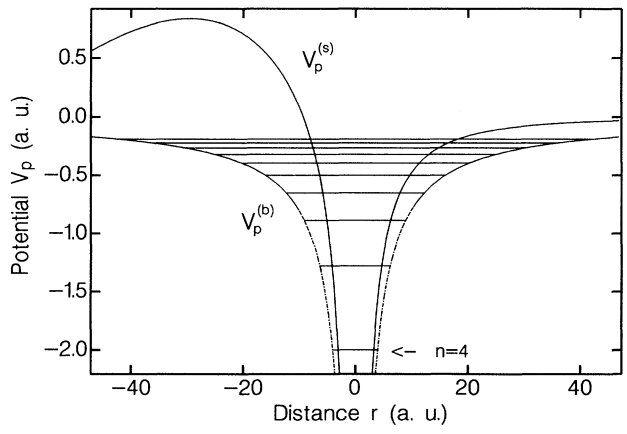

FIG. 1. Bare Coulomb potential $V_p^{(b)}$ and screened Coulomb potential $V_p^{(s)}$ for a 2-MeV/u O^{8+} ion traversing a thick carbon foil. $V_p^{(s)}$ is calculated in linear response theory [11]. The quantum-mechanical energy levels are indicated by horizontal lines.

The transport problem is solved by Monte Carlo sampling of a discrete ensemble of initial phase-space coordinates which are propagated according to Eq. (2). For a more detailed description of the transport model we refer to Ref. [8].

B. Initial conditions

In this work we are interested in studying the production of O^{7+} ions in Rydberg states resulting from the interaction of 2-MeV/u O^{2+} ions with a thick carbon foil. The charge-state distribution for this collision system is in complete equilibrium after passing through a carbon foil of 20 $\mu g/cm^2$, the most probable charge states being O^{7+} and O^{8+}. Therefore, the initial electronic phase-space distribution at each target thickness is generated by a thickness-independent source of primary collision events, in which an electron is either captured from a target atom or excited from a low-lying bound state of O^{7+}.

These initial electronic conditions are chosen to closely resemble the result of fast binary collisions between the projectile and the target. Unfortunately, the choice of these initial conditions is not unique since it requires the knowledge of the initial phase-space distribution as a function of six dynamical variables, i.e., $P_0(\mathbf{r},\mathbf{v})$ or, equivalently, $P_0(E,l,\psi,\alpha,\beta,\gamma)$ where (α,β,γ) are the Euler angles describing the orientation of the orbit in a space-fixed frame and ψ is the mean anomaly describing the instantaneous position on the orbit. This information cannot be uniquely obtained experimentally (e.g., from measured cross sections) since, according to the uncertainty principle, the maximum set of compatible observables (i.e., quantum numbers) for the present case is equal to 3: e.g., (n,l,m) or equivalently (E,l,m). Alternatively, an attempt could be made to obtain the initial conditions from quantum-mechanical pseudo-phase-space distributions (e.g., Wigner functions) obtained from the wave function after the binary collision between the target and the projectile. However, this procedure would not only be a formidable task, but it is also not uniquely defined and possesses inherent limitations in the compatibility of quantum-mechanical and classical phase-space distributions.

In view of these ambiguities in the definition of the initial conditions, and to study the dependence of the final results on the particular choice made for these conditions, we consider in this work two different initial phase-space distributions. The simplest one will be named "random" and will be denoted by $P_{\text{random}}(E,l,\psi,\alpha,\beta,\gamma)$. This distribution is assumed to be spatially isotropic, which implies that all Euler angles are uniformly randomized on the unit sphere. In addition, the mean anomaly is assumed to be uniformly distributed in the interval $[-\psi_0,\psi_0]$ with $\psi_0 \leq \pi$. The limit ψ_0 corre-

sponds to a maximum distance $|r(\psi_0)| \geq r_0$ from the projectile nucleus, which is a maximum radius outside of which the primary collision events cannot occur. An estimate for r_0 can be derived from three increasingly restrictive criteria: (i) r_0 should be smaller than the dynamical screening length ($r_0 < \lambda_D = v_p/\omega$, ω being the plasma frequency), (ii) r_0 should not exceed the maximum distance from the nearest atom in the solid ($r_0 < r_{WS}$, where r_{WS} is the Wigner-Seitz radius), and (iii) r_0 should be of the order of the impact parameter for an electron-ion collision sufficient to transfer a momentum to the electron of the order of v_p ($r_0 \lesssim 2Z_p/v_p^2$). For the present study, we have chosen a value for r_0 corresponding to the intermediate criteria (ii), i.e., $r_0 \approx 2.2$ a.u. Finally, the energy and angular-momentum distributions are taken from known cross sections for the formation of Rydberg states in ion-atom collisions. For the energy distribution $D(E)$ we have chosen $D(E) = \text{const}$, or equivalently, an n distribution following an n^{-3} law, which is a well- known result for Rydberg states at high collision speeds. Considering that in the present work we are only interested in the production of Rydberg states and taking into account the condition given by Eq. (1), we have restricted the range of $D(E)$ to an energy band of -4 a.u. $\leq E \leq 4$ a.u. in the projectile frame. The choice of a cutoff on the high-energy side is based on the fact that electrons with high relative speeds $|\mathbf{v}_e - \mathbf{v}_p|$ escape very quickly from the immediate neighborhood of the projectile ion. Their chance to be recaptured into a Rydberg bound state via inelastic or elastic collisions in the solid (Coulomb trapping [8]) is therefore very small. On the other hand, the l distribution is taken from calculated cross sections for the production of excited projectile states in ion-atom collisions. For the present case, these distributions have been obtained from the CTMC calculation described below. In summary, the "random" initial distribution represents the maximum randomness or maximum-entropy distribution for classical variables subject to the constraints provided by known properties of ion-atom collisions. It should be stressed that this distribution is not microcanonical, since the latter would correspond to an unconstrained maximum randomness for each energy shell.

An improved initial phase-space distribution can be achieved using the CTMC method [13]. Details of the CTMC model used in this work can be obtained from the article of Toburen *et al.* [14]. The CTMC method has two major advantages: it takes the collision dynamics explicitly into account and gives realistic estimates for the initial population of excited states after a binary collision. Furthermore, it generates directly the six-dimensional phase-space distributions, avoiding any hypothesis about the randomization at this stage. The initial distribution $P_0(\mathbf{r},\mathbf{v})$ is obtained by integrating the trajectory of each individual electron up to a separation of 10 a.u. between projectile and target in the direction of $\mathbf{v}_p$. At this point, the influence of the target atom on electrons in the energy band -4 a.u. $\leq E \leq 4$ a.u., which is not considered in the transport code, can be neglected. On the other hand, the distance of propagation must be chosen small enough so that the probability for the electron to suffer an inelastic or elastic collision is small. The latter requirement is certainly fulfilled for the collision system studied here since the mean free path for inelastic scattering and elastic scattering are $\lambda_i \approx 51$ a.u. and $\lambda_e \approx 50$ a.u., respectively.

For the present system, we have found that the major contribution to the production of electrons in the energy band mentioned above are the electron capture from the K shell of C and the excitation from the $n=1$ and $n=2$ shells of O^{7+} with cross sections σ_{cap}, $\sigma_{exc}^{(1)}$, and $\sigma_{exc}^{(2)}$. These cross sections are weighted with the equilibrium charge-state fraction of O^{8+}, F_8, $O^{7+}(n=1)$, $F_7^{(1)}$, and $O^{7+}(n=2)$, $F_7^{(2)}$ to determine the relative sizes of the ensembles of initial conditions associated with each case. The fraction of the $n=2$ shell of oxygen was estimated by using an n^{-3} dependence for the relative occupation. With the relation

$$N_{cap} = \frac{\sigma_{cap}F_8}{\sigma_{exc}^{(1)}F_7^{(1)}} N_{exc}^{(1)} = \frac{\sigma_{cap}F_8}{\sigma_{exc}^{(2)}F_7^{(2)}} N_{exc}^{(2)} \tag{3}$$

we obtained the relative fraction of captured (N_{cap}) and excited ($N_{exc}^{(1)}$ and $N_{exc}^{(2)}$) electrons which are listed in Table I. More than 60% of the initial phase-space distribution arises from capture. The resulting energy distribution $D(E)$ in the projectile frame is displayed in Fig. 2 (denoted as CTMC initial distribution) and shows a slow decrease as a function of the electron energy E. This behavior differs slightly from the $D(E) = \text{const}$ assumption made for the random initial phase-space distribution (denoted as random initial).

The initial n,l distribution resulting from the CTMC calculations for a variety of different n shells is given in Fig. 3. As expected from binary ion-atom collision theory, all distributions are peaked at low-l values ($l \approx 1$). However, it is a remarkable fact that no significant change as a function of n can be observed, i.e., the n,l distribution appears to be separable. This separability is very important in view of the task of modeling realistic random initial phase-space distributions and it drastically simplifies the determination of the initial l distribution.

For a better understanding of the similarities and differences between the CTMC phase-space distributions and the random initial distributions it is instructive to study projections of the distribution functions. A projection of the initial space coordinates onto an arbitrary plane in the coordinate space would result in a structureless cloud of points around the projectile nucleus. A more "orderly" picture can be obtained when all the

TABLE I. Equilibrium charge-state distributions for O^{8+}, F_8, $O^{7+}(n=1)$, $F_7^{(1)}$, and $O^{7+}(n=2)$, $F_7^{(2)}$ for O^{2+} (2 MeV/u)$\rightarrow$ carbon foil. Also given are CTMC cross sections for capture and excitation from the $n=1,2$ shell of O^{7+} into an energy band -4 a.u. $\leq E \leq 4$ a.u. N denotes the percentage of initial conditions associated with each process.

Process	F_q	σ (cm^2)	N (%)
$O^{8+} \rightarrow C(K)$	0.320	3.13×10^{-18}	62
$O^{7+}(n=1) \rightarrow C$	0.444	3.28×10^{-19}	9
$O^{7+}(n=2) \rightarrow C$	0.055	8.38×10^{-18}	29

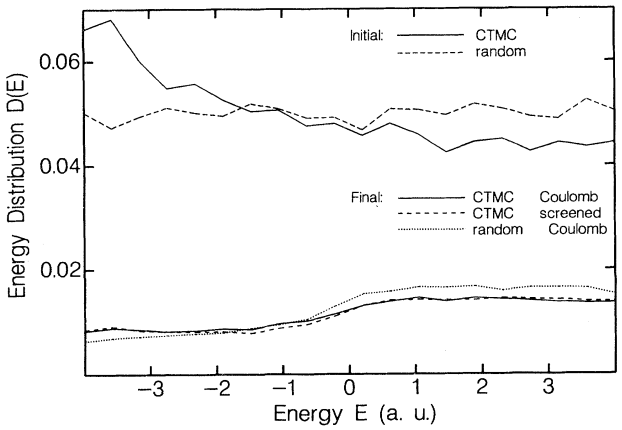

FIG. 2. Energy distribution $D(E)$ in the interval -4 a.u. $\leq E \leq 4$ a.u. before (top) and after (bottom) transport averaged over all target thicknesses. Initial distributions are displayed for CTMC or random initial conditions. Final distributions are shown for different combinations of initial conditions and evolution in different projectile potentials (Coulomb or screened Coulomb field).

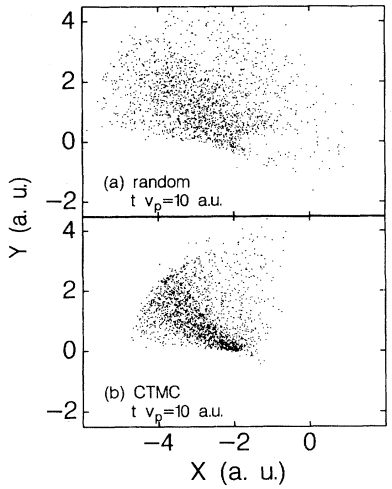

FIG. 4. Evolution of the initial coordinate-space distributions for a random distribution (a) and a CTMC distribution (b) up to a separation of $tv_p = 10$ a.u. between target and projectile.

different orbits, whose orientations are characterized by the Euler angles α,β,γ, are rotated into a single orbital x-y plane, which is defined by the angular-momentum vector **L** pointing in the z direction (out of the plane in Fig. 4) and the pericenter vector, pointing in the positive x direction. In this representation, all unperturbed Coulomb orbits are symmetric with respect to the x axis and electrons in the continuum escape in the direction of negative x values.

The space coordinates for the initial random distribution are calculated for the moment of closest approach between projectile and target, denoted as $t = 0$. In order to compare them with the initial CTMC distribution we can either evolve the random initial conditions in time to match the CTMC values at $tv_p = 10$ a.u., or evolve the CTMC data back to $t = 0$, in the absence of the target. In Fig. 4 the random distribution is shown together with the CTMC initial space distribution for $tv_p = 10$ a.u. In both cases most of the electrons are found in the upper left part of the figure, signifying that they already passed the pericenter and are heading away from the projectile ion. No dramatic difference between the two distributions is visible. Slight differences become evident when we evolve the positions of all CTMC initial conditions back to point of closest approach between target and projectile ion (Fig. 5). The major part of all electrons is confined to a very small volume element. The random distribution in Fig. 5(a) again looks very similar to the CTMC initial distribution although the electrons are spread over a larger

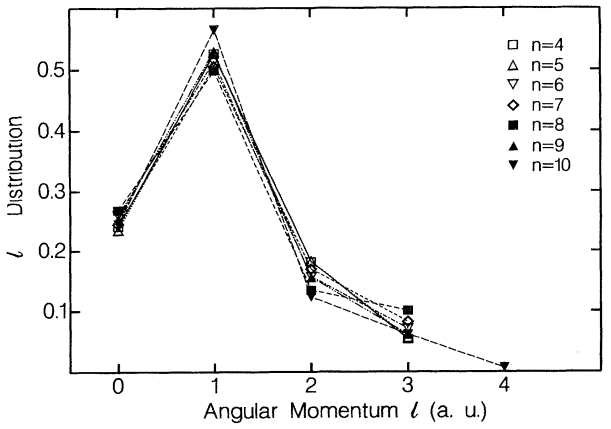

FIG. 3. Initial n,l distribution calculated with the CTMC method (sum over l normalized to 1 for each n).

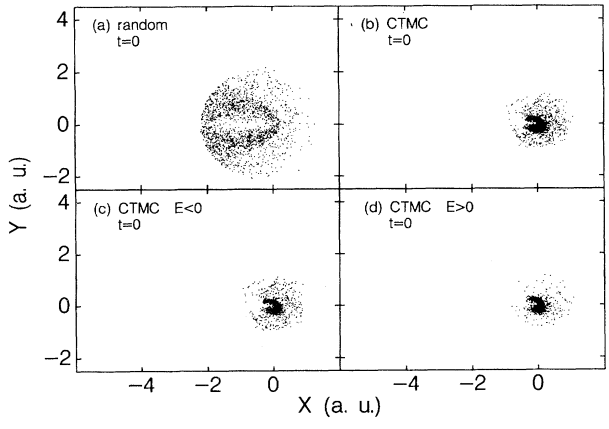

FIG. 5. Initial coordinate-space distributions from a random distribution (a) and a CTMC distribution (b) evolved back in time to $t = 0$. In (c) and (d) the CTMC coordinate-space distributions at $t = 0$ are decomposed in bound (c) and free electrons (d).

volume. The latter is due to the choice of $r_0=2.2$ a.u., which indicates that the most restrictive criterion (iii) discussed above is better in line with the CTMC calculations.

The empty region close to the nucleus in Figs. 5(a) and 5(b) is due to the restriction $E \geq -4$ a.u. Deeply bound states, which would be located closer to the origin, are not occupied. The CTMC initial distribution in Fig. 5(b) is symmetrically distributed around the pericenter.

Additionally, in Figs. 5(c) and 5(d) the CTMC initial conditions are decomposed into bound electrons [5(c)] and free electrons [5(d)], respectively. Between these two distributions no apparent difference is visible. This indicates that the large momentum transfer required for capture into highly excited or low-lying continuum states smears out any difference between these two regimes. Accordingly, electrons in those states originate from the same initial coordinate-space region.

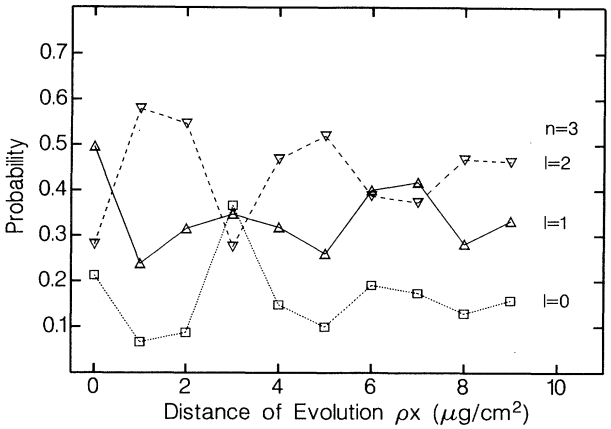

FIG. 6. Stark-induced l mixing for the $n=3$ level of O^{7+} in a dynamically screened Coulomb field (wake potential).

C. Stark mixing in the dynamical screened potential

The time evolution resulting from the Langevin equation [Eq. (2)] takes into account two different processes: on one hand, inelastic- and elastic-scattering events of electrons with electrons and atoms in the solid described by the stochastic force $\mathbf{F}(t)$, which is modeled after known scattering cross sections for free electrons in solids [8]; on the other hand, the evolution of the electron in the field $V_p(\mathbf{r})$ of the projectile ion. Therefore, it is of interest to test the sensitivity of the evolution to the form of this field. For example, some differences should be expected when the evolution is evaluated by means of either a bare Coulomb field $V_p^{(b)}(\mathbf{r})$ or a dynamically screened Coulomb field $V_p^{(s)}(\mathbf{r})$ (see Fig. 1) which contains an electric field ("wake" field) at small distances from the nucleus. In fact, Rozet *et al.* [15] observed n,l distributions in low-lying n states of krypton ions ($n=2$) which they could explain in terms of Stark field mixing in the screened potential. Also, recent calculations of Müller *et al.* [12] show that—in the absence of inelastic and elastic scattering—the anisotropic screening of the Coulomb potential not only leads to a periodic fluctuation in l as a function of time, but also shows in the limit of strong perturbation an effective l mixing by l diffusion to higher-l states.

In Fig. 6 we display the time evolution of the l distribution for the $n=3$ level of O^{7+} in a dynamically screened potential *in the absence of inelastic- and elastic-scattering events.* As a result of the anisotropic screening, the initial l distribution, taken from the CTMC result for binary ion-atom collisions, is seen to oscillate and to eventually lead to an appreciable change in the overall l distribution. This type of l mixing might be expected to have some effect on the l distribution arising from the transport problem. However, we have found that these "quantum beats" (in fact, classical beats) are of minor influence on the final outcome of our classical transport calculation for high Rydberg states. A simple estimate based on scaling properties of collisional cross sections and Stark splitting [12] indicates that with increasing n, collisional l mixing dominates over Stark mixing of l. Nevertheless, the effect of additional l mixing will be tested below.

D. Surface effects

Before an excited state can be observed, the projectile ion has to pass through the solid-vacuum boundary at the exit surface of the target. In the velocity regime studied here, electron kinetic energies relative to the target exceed several hundreds of eV. Comparing these kinetic energies to the height of the surface barrier (≈ 5 eV), it can be concluded that surface effects including projectile-induced dynamical image charges can be neglected [16]. On the other hand, the transition from a screened Coulomb field inside the solid to an unscreened field after emerging from the surface leads to a repartition of the energy distribution in a shake-down-like transition which conserves the angular momentum l. This redistribution is taken explicitly into account in the simulation. Additional Stark mixing due to the image potential near the exit surface can be neglected at high velocities but could be taken into account for large Sommerfeld parameters $Z_p/v_p \gg 1$.

E. Final angular-momentum distributions

Because the phase-space energies of bound states are continuous, it is necessary to assign a definite band of final binding energies E to a given quantum-mechanical n level. Here, the range of E values associated with an n level is assumed to be $n-\frac{1}{2} \leq (-2E/Z_p^2)^{1/2} \leq n+\frac{1}{2}$. For similar reasons, a band of angular momenta $l \leq L \leq l+1$ is assigned to the quantum number l. In the limit of large quantum numbers (i.e., Rydberg states) these two assignments reproduce the correct quantum-mechanical weights and mean values associated with each n,l sublevel.

In the bulk of the solid, electrons are continuously excited from low-lying bound projectile states or captured from target atoms. The final l distributions are therefore the result of an average over electrons originating from

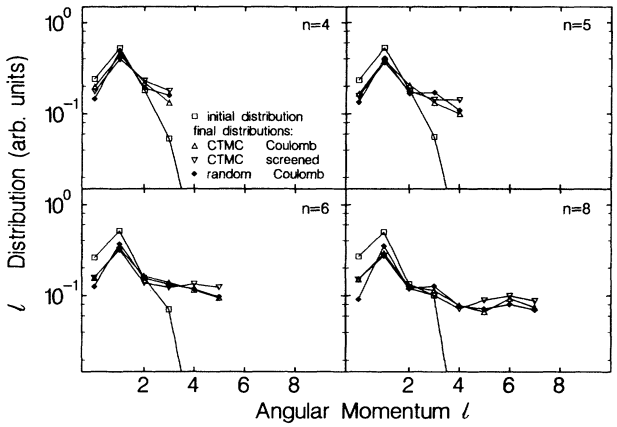

FIG. 7. Calculated l distributions for the $4 \leq n \leq 8$ shells of 2-MeV/u O^{7+} ions before and after passage through a 1000-a.u. (≈ 10-$\mu g/cm^2$) thick carbon foil.

different depths inside the target. In Figs. 7 and 8 we display the final l distributions for different n levels of O^{7+} after traversing a target thickness of 1000 a.u. (approximately 10 $\mu g/cm^2$) which is sufficiently large to obtain complete equilibrium. The initial l distributions obtained from CTMC calculations are also shown. For low-n values, the overall shape of the curves still resembles the initial distribution. However, an onset of a shift to higher-l states becomes visible. For higher-n values we observe a sharp contrast to the CTMC initial distributions. The l distribution is composed of two components: a contribution similar to the initial distribution accentuating low-l values and a slowly decreasing tail extending to very-high-l values. The low-l part stems from electrons excited in the last layers of the target whereas the high-l part represents those electrons from deep inside the bulk.

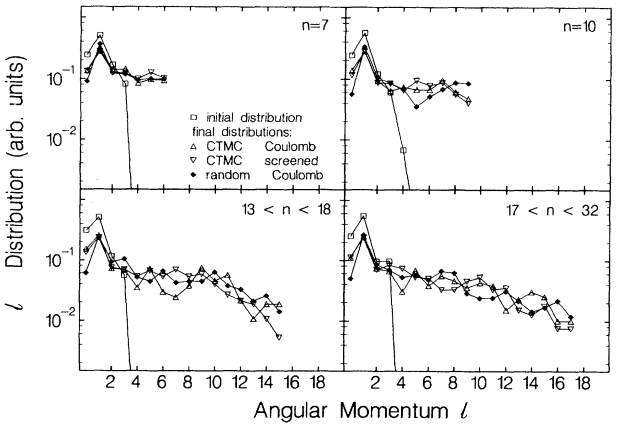

FIG. 8. Calculated l distributions for the $7 \leq n \leq 32$ shells of 2-MeV/u O^{7+} ions before and after passage through a 1000-a.u. (≈ 10-$\mu g/cm^2$) thick carbon foil. Several n shells had to be summed up to get reasonable statistics.

While the initial CTMC distributions contrast sharply with the final distributions after transport, the difference between the l distribution for transport in a bare Coulomb and in a screened Coulomb field is remarkably small. Only for low-lying n shells a slight enhancement towards high-l values can be seen for the evolution in a screened Coulomb field. This is in line with the l mixing due to the wake field discussed above. However, the statistical error due to the Monte Carlo method does not allow proof of the existence of this rather small effect.

III. CASCADE CALCULATION

In order to compare our n,l distribution with experiment, we have calculated the cascade evolution subsequent to the ion-solid collision of the highly excited states down to the $2p$ and $3p$ levels whose Lyman transitions to the $1s$ state have been experimentally observed [7]. Denoting the level population by N_{nl} and the transition probability by $A_{nl,n'l'}$ we can write the differential change of this population as

$$\frac{dN_{nl}(t)}{dt} = \sum_{i=N+1}^{\infty} N_{il\pm1}(t) A_{il\pm1,nl} - N_{nl}(t) \sum_{j=1}^{n-1} A_{nl,jl\pm1} , \tag{4}$$

where the transition probabilities $A_{nl,n'l'}$ for a one-electron system can be taken from Ref. [17]. This system of coupled rate equations has been solved numerically for a large number of states (≈ 450) and the photon intensities for $Ly_\beta(3p-1s)$ and $Ly_\alpha(2p-1s)$ decay have been calculated as $I_{3p-1s}(t) = N_{3p}(t) A_{3p,1s}$ and $I_{2p-1s}(t) = N_{2p}(t) A_{2p,1s}$, respectively.

It has been found experimentally [2,3,18,5,7] for very different collision systems that these intensities as a function of time obey a power law of the form t^{-a} with $a \approx 1.5$. In several papers [19,18] an attempt has been made to derive this power-law dependence from general assumptions for the n,l distribution before the cascading. To get a more quantitative understanding of the influence of the population of cascading Rydberg states on the photon intensities, we compare in Fig. 9 these intensities for two different n,l distributions: the one resulting from a binary collision and the one arising from our transport simulation (i.e., from Figs. 7 and 8). The slope of the Ly_β intensity for these two cases is found to be similar whereas the slope of the Ly_α intensity is very different. The reason is that low-l states feed with approximately equal contributions the $3p$ and $2p$ levels, whereas high-l states mostly decay via the yrast sequence to the $2p$ state [18]. Therefore, the weaker decrease in the Ly_α intensity for $t > 0.3$ ns can be attributed to the lack of high-l states in binary collisions. Differences are also appreciable in the intensity ratio of Ly_α to Ly_β radiation. The reason for this difference is again the lack of supply from higher-l states feeding preferentially the $2p$ state. Figure 9 indicates that the ratio of the Ly_α to Ly_β emission is a very sensitive measure for the population of high-l states.

It has been previously pointed out [18] that the highest n level included in the cascading process determines the time interval in which the power-law dependence is

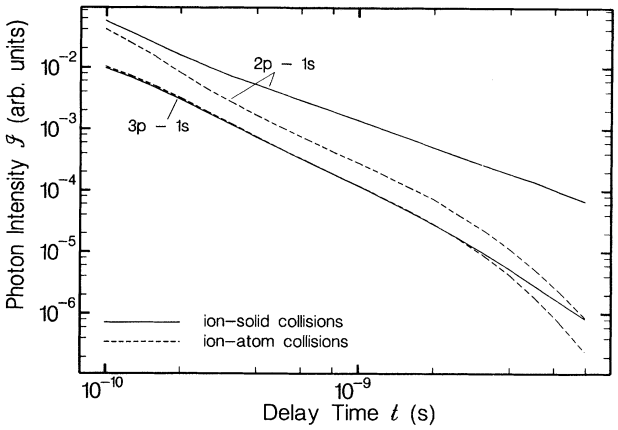

FIG. 9. Calculated delayed photon emission intensities resulting from binary ion-atom collisions (dashed line) and from transport simulation (solid line).

fulfilled. Furthermore, it gives an estimate of the n state up to which the experiment should be sensitive. Accordingly, since we include only states $n \leq 30$ in the cascade calculations we observe a rapid drop of intensity for $t > 4$ ns.

IV. COMPARISON WITH EXPERIMENT

In Fig. 10 the calculated delayed photon intensity is displayed for the n,l distributions arising from different model assumptions. Within the statistical error of the Monte Carlo simulation, all model calculations show excellent agreement with the experimental data of Can *et al.* [7]. It is apparent that the common factor in the different model calculations, i.e., the multiple scattering described by a stochastic sequence of collisions, is much more important than the evolution of the electron in a bare or screened Coulomb potential. As expected from the similarity of the initial distributions, the results for CTMC and random initial conditions do not differ significantly. This result also shows that the statistical fluctuations of the high-l distributions are smoothed out by the cascading process and do not influence measurably our final result.

The largest deviation from experiment in Fig. 10 (still within the statistical error) is found for the cascade intensity resulting from the random initial distribution. This can be traced to the slight differences in the final energy distribution [$D(E)$ in Fig. 2] which in turn are due to the slight deviation of the CTMC initial energy distribution from the distribution $D(E)$=const assumed in the random initial model. The different energy distributions translate into different n distributions. In a model for the cascade process Hopkins and von Bretano [19] have shown that the exponent in the power-law dependence for the photon flux depends sensitively on the population of the n states.

In Fig. 11 the ratio of Ly_α to Ly_β intensity is displayed. Most striking is the difference between the result from binary ion-atom collisions and the transport simulation, which amounts to more than a factor of 4. This difference demonstrates convincingly the importance of stochastic multiple scattering inside the solid. In contrast, deviations among the different transport simulations are small. Within the experimental error, all agree with experiment for both the absolute magnitude and the slope as a function of delay time t. The sensitivity of the ratio $I_{Ly_\alpha}/I_{Ly_\beta}$ can be estimated when the result in Fig. 11 is compared to a calculation made in the paper of Can

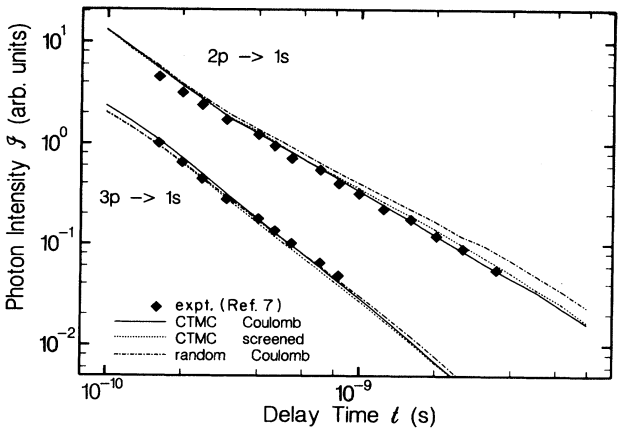

FIG. 10. Calculated delayed photon emission intensity for different model assumptions in the transport simulation together with the experimental results of Can *et al.* [7] (rhombi). The transport calculations with CTMC initial conditions have been performed using a bare Coulomb field (solid line) and a screened Coulomb field (dotted line). The random initial distribution has been evolved in a Coulomb field (dash-dotted line).

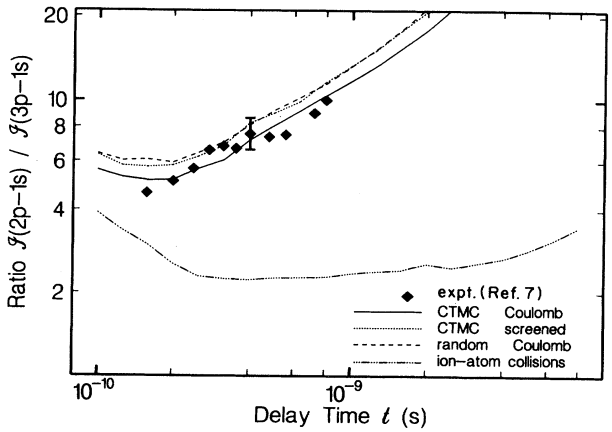

FIG. 11. Ratio of the calculated Ly_α to Ly_β intensity together with the experimental results of Can *et al.* [7] (rhombi). The different models include transport simulations with CTMC initial conditions evolved in a bare Coulomb field (solid line) and in a screened Coulomb field (dotted line) and also a random initial distribution evolved in a Coulomb field (dashed line). The result from binary ion-atom collisions is also displayed (dash-dotted line).

et al. [7] assuming a constant l distribution. Although such a distribution is seemingly similar to those shown in Figs. 7 and 8, the calculated ratio is 20% higher than the experimental result and therefore far outside the experimental uncertainty.

Since the effect of stochastic scattering events in a solid on the final n and l distributions is very similar for different projectile ions and the transition probabilities for hydrogenic ions scale uniformly with the fourth power of the ion charge, we can expect that in different collision systems the time dependence of the Ly_α and Ly_β intensities should closely resemble the one calculated here, except for rescaling the time scale by Z_p^{-4}. This has been indeed experimentally verified in several experiments [2,3,18,5,7].

V. CONCLUSIONS

The classical transport calculation treating multiple scattering in a solid can successfully describe the formation of Rydberg states with very high angular momenta. Simulating the post-foil-interaction cascade processes, we find good agreement with experimental data obtained with delayed-photon-emission spectroscopy. Our calculations clearly indicate that the most important factor forming high-l states is the stochastic scattering of the highly excited electrons in the solid, whereas l mixing due to Stark splitting is of minor importance. Furthermore, we find that for high-n values the results are, to a good approximation, independent from the details of the chosen either random or CTMC initial conditions.

ACKNOWLEDGMENTS

This work was supported in part by DFG/Bonn, the NSF and by the U.S. DOE under Contract No. DE AC05-84OR21400 with Martin Marietta Energy Systems, Inc.

[1] W. S. Bickel and A. S. Goodman, Phys. Rev. **148**, 1 (1966).
[2] P. Richard, Phys. Rev. Lett. **45A**, 13 (1973).
[3] W. J. Braithwaite, D. L. Matthews, and C. F. Moore, Phys. Rev. A **75**, 465 (1975).
[4] H. D. Betz, D. Röschenthaler, and J. Rothermel, Phys. Rev. Lett. **50**, 34 (1983).
[5] J. Rothermel, H. D. Betz, and F. Bell, Nucl. Instrum. Methods **194**, 341 (1982).
[6] Y. Yamazaki, N. Stolterfoht, P. D. Miller, H. F. Krause, P. L. Pepmiller, S. Datz, I. A. Sellin, J. N. Scheurer, S. Andriamonje, D. Bertault, and J. F. Chemin, Phys. Rev. Lett. **61**, 2913 (1988).
[7] C. Can, R. J. Maurer, B. Bandong, and R. L. Watson, Phys. Rev. A **35**, 3244 (1987).
[8] J. Burgdörfer in *Proceedings of the Third Workshop on High Energy Ion-Atom Collisions,* edited by D. Berényi and G. Hock, Lecture Notes in Physics Vol. 294 (Springer-Verlag, Berlin, 1988), p. 344; J. Burgdörfer in *Proceedings of the Sixteenth International Conference on the Physics of Electronic and Atomic Collisions, New York, 1989,* AIP Conf. Proc. No. 205, edited by A. Dalgarno, R. S. Freund, M. S. Lubell, and T. B. Lucatorto (AIP, New York, 1990); J. Burgdörfer and J. Gibbons, Phys. Rev. A **42**, 1206 (1990).
[9] J. Burgdörfer and C. Bottcher, Phys. Rev. Lett. **61**, 2917 (1988).
[10] J. Burgdörfer, in *Proceedings of the 4th Workshop on High-Energy Ion-Atom Collision Processes,* edited by D. Berényi and G. Hock, Lecture Notes in Physics Vol. 376 (Springer-Verlag, Berlin, 1991), p. 199.
[11] P. M. Echenique, R. H. Ritchie, and W. Brandt, Phys. Rev. B **20**, 2567 (1979).
[12] J. Müller and J. Burgdörfer, Phys. Rev. A **41**, 4903 (1990).
[13] R. Abrines and I. C. Percival, Proc. Phys. Soc. London **88**, 861 (1966); R. E. Olson and A. Salop, Phys. Rev. A **16**, 531 (1977).
[14] L. H. Toburen, R. D. Dubois, C. O. Reinhold, D. R. Schultz, and R. E. Olson, Phys. Rev. A **42**, 5338 (1990).
[15] J. P. Rozet, A. Chetioui, C. Stephan, A. Touati, D. Verhet, and K. Wohrer, in *Proceedings of the Third Workshop on High Energy Ion-Atom Collisions,* edited by D. Berényi and G. Hock, Lecture Notes in Physics Vol. 294 (Springer-Verlag, Berlin, 1988), p. 307.
[16] J. Burgdörfer, Nucl. Instrum. Methods **202**, 253 (1982).
[17] H. A. Bethe and E. E. Salpeter, *Quantum Mechanics of One- and Two-Electron Atoms* (Plenum, New York, 1977).
[18] H. D. Betz, J. Rothermel, and F. Bell, Nucl. Instrum. Methods **170**, 243 (1980).
[19] F. Hopkins and P. von Bretano, J. Phys. **B9**, 775 (1976).